High-contrast electro-optic modulation of spatial light induced by graphene-integrated Fabry–Pérot microcavity

Article *in* Applied Physics Letters · September 2014

DOI: 10.1063/1.4895633

CITATIONS
75

READS
310

3 authors, including:

Chao Zeng
Chinese Academy of Sciences
39 PUBLICATIONS **858** CITATIONS

SEE PROFILE

High-contrast electro-optic modulation of spatial light induced by graphene-integrated Fabry-Pérot microcavity

Chao Zeng, Jing Guo, and Xueming Liu

Citation: Applied Physics Letters **105**, 121103 (2014); doi: 10.1063/1.4895633
View online: http://dx.doi.org/10.1063/1.4895633
View Table of Contents: http://scitation.aip.org/content/aip/journal/apl/105/12?ver=pdfcov
Published by the AIP Publishing

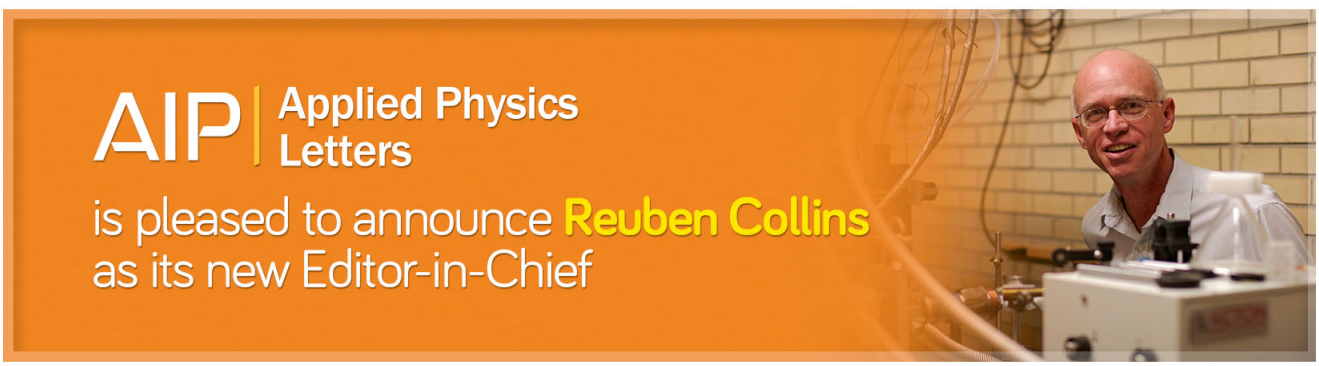

High-contrast electro-optic modulation of spatial light induced by graphene-integrated Fabry-Pérot microcavity

Chao Zeng,[a] Jing Guo,[a] and Xueming Liu[b]
State Key Laboratory of Transient Optics and Photonics, Xi'an Institute of Optics and Precision Mechanics, Chinese Academy of Sciences, Xi'an 710119, China

(Received 21 July 2014; accepted 29 August 2014; published online 22 September 2014)

We have proposed a graphene-integrated Fabry-Pérot microcavity for efficient modulation of spatial light. A simplified theoretical model is established to analyze the performance of our system, and the calculated results agree well with the simulation results. It is shown that the plasmon-induced transparency (PIT) effect is achieved in the proposed microcavity and the central frequency of PIT window can be dynamically tuned by gate voltages. In particular, the PIT spectra exhibit extremely large modulation depths (~90%) across a broad range of frequencies. The proposed ultracompact configuration demonstrates a type of cavity-induced high-contrast and frequency-selective electro-optic modulators, offering opportunities in exploiting active chip-integrated high-performance devices operating at frequencies from terahertz to mid-infrared. © *2014 AIP Publishing LLC*.
[http://dx.doi.org/10.1063/1.4895633]

Graphene, a monolayer of sp^2-hybridized carbon, has evolved into a thriving research hotspot since the first achievement of remarkably high-quality graphene by Novoselov *et al.* in 2004.[1–3] Due to its exceptionally high carrier mobility and tunability via external fields, a variety of graphene-based optoelectronic devices have been explored such as electro-optical modulators[4,5] and photodetectors.[6,7] A pristine single-layer graphene exhibits a nonresonant absorption of 2.3% across the infrared and visible ranges, which is so weak as to limit the modulation strength and photoresponsivity of devices.[4,7,8] To date, several approaches have been exploited to enhance the performances of graphene-based devices as diverse as employing total internal reflections,[9,10] integrating graphene with photonic microcavities/metamaterials,[11,12] and patterning graphene into plasmonic resonators.[13–17] Because of their excellent resonance characteristics and flexible tunability, graphene plasmonic nanostructures exhibit great potential in strongly manipulating the spatial light in active chip-integrated photonic circuits.[18] For instance, Tian *et al.* first demonstrated the plasmon-induced transparency (PIT) effect in periodically patterned graphene nanostrips.[17] In their planar graphene-based metamaterials, a ~30% amplitude modulation based on PIT effect was achieved in the mid-infrared region. However, large modulation-depth and frequency-selective modulation of spatial light remain a challenge.

In this letter, we propose a graphene-integrated Fabry-Pérot (FP) microcavity to efficiently modulate the spatial light. Theoretical analyses and numerical simulations show that the dynamically tunable PIT effect can be realized in our system due to the joint effect of graphene plasmon resonances and FP oscillations. Significantly, the modulation depth can reach ~90% across a broad range of frequencies. By taking advantages of the PIT effect, the proposed graphene-integrated FP microcavity may find potential applications in active chip-integrated high-performance modulation devices.

As shown schematically in Fig. 1(a), the proposed graphene-integrated FP microcavity consists of two graphene ribbon arrays (GRAs) spatially separated by a dielectric (SiO_2) spacer. The carrier concentration in GRAs is

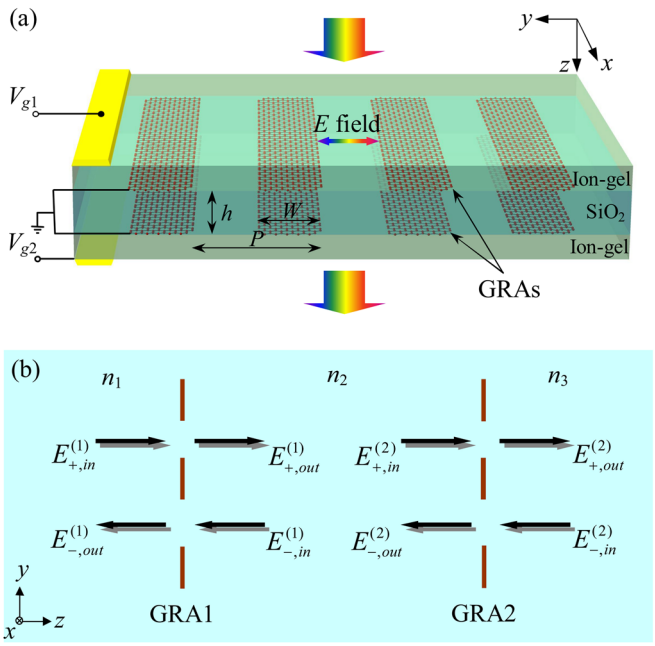

FIG. 1. (a) Schematic of the graphene-integrated FP microcavity consisting of two GRAs spatially separated by a SiO_2 ($n_2 = 1.45$) spacer. The Fermi energy in GRAs is tuned by using the ion-gel ($n_1 = n_3 = 1.35$) gates through two gate voltages V_{g1} and V_{g2}. The separation of two GRAs, ribbon width, and period of GRAs are denoted by h, W, and P, respectively. The excitation wave along $+z$-axis direction is linearly polarized with the electric field vector perpendicular to the ribbons. (b) Transfer matrix model of the FP microcavity formed between GRA1 and GRA2. The electric field vectors of incident and output waves at GRA1 (superscript "1") and GRA2 (superscript "2") are marked by subscripts "in" and "out," respectively. The electric field vectors with subscripts "+" and "−" represent the field propagating along $+z$-axis and $-z$-axis directions, respectively.

[a]C. Zeng and J. Guo contributed equally to this work.
[b]Author to whom correspondence should be addressed. Electronic mail: liuxm@opt.ac.cn

controlled by using the ion-gel gates through electrostatic gating, and hence the optical transmission of the system is modulated by gate voltages V_{g1} and V_{g2}.[13] A linearly polarized (perpendicular to the ribbons) mid-infrared wave incident along $+z$-axis direction is employed to excite plasmon oscillations in GRAs.[13,14] The dynamic transmission is here evaluated by employing graphene plasmons and transfer matrix theory.[5,13,14] Figure 1(b) illustrates the transfer matrix model of the proposed FP microcavity with two spatially separated conductive media (i.e., GRA1 and GRA2) represented by matrices M_1 and M_2, respectively. The relationship between electric field vectors of the incident and emergent waves is simplified as[19,20]

$$\begin{pmatrix} E^{(2)}_{+,out} \\ E^{(2)}_{-,in} \end{pmatrix} = M_2 \begin{pmatrix} e^{i\varphi} & 0 \\ 0 & e^{-i\varphi} \end{pmatrix} M_1 \begin{pmatrix} E^{(1)}_{+,in} \\ E^{(1)}_{-,out} \end{pmatrix}, \qquad M_j = \frac{1}{t_{21}} \begin{pmatrix} t_{12}t_{21} - r_{12}r_{21} & r_{21} \\ -r_{12} & 1 \end{pmatrix}. \tag{1}$$

Here, the Fresnel coefficients for normal incidence in matrix M_j $(j = 1, 2)$ are governed by[21]

$$t_{12} = \frac{2n_j}{n_j + n_{j+1} + Z_0\sigma_j}, \quad t_{21} = \frac{2n_{j+1}}{n_j + n_{j+1} + Z_0\sigma_j}, \quad r_{12} = \frac{n_j - n_{j+1} - Z_0\sigma_j}{n_j + n_{j+1} + Z_0\sigma_j}, \quad r_{21} = \frac{n_{j+1} - n_j - Z_0\sigma_j}{n_j + n_{j+1} + Z_0\sigma_j}. \tag{2}$$

The refractive indices of three dielectric layers are $n_1 = n_3 = 1.35$ (ion-gel) and $n_2 = 1.45$ (SiO_2).[11,13,16] $\varphi = n_2 h\omega/c$ is the phase difference between two GRAs, ω is the angular frequency of incident wave, and c is the speed of light in vacuum. $Z_0 = 376.73\ \Omega$ is the vacuum impedance. Under conditions of the quasistatic approximation and neglecting lateral ribbon-ribbon interaction, the average sheet optical conductivity σ_j of GRAs is given by[14]

$$\sigma_j(\omega) = i\frac{fD_j}{\pi} \frac{\omega}{(\omega^2 - \omega_{p,j}^2) + i\Gamma_{p,j}\omega}, \tag{3}$$

where $D_j = e^2 E_{F,j}/\hbar^2$ is the Drude weight, e is the electron charge, $E_{F,j}$ is the Fermi energy of GRA1 $(j = 1)$ and GRA2 $(j = 2)$, and $\hbar$ is the reduced Planck's constant. $\Gamma_{p,j}$ is the plasmon resonance width of GRAs, which is usually 10% larger than the Drude scattering width $\Gamma_j = e{v_F}^2/(\mu E_{F,j})$ in the unpatterned graphene. $v_F \approx c/300$ is the Fermi velocity. Here, the measured DC mobility $\mu = 10\,000\ \mathrm{cm^2\ V^{-1}\ s^{-1}}$ is chosen to perform the investigations.[1,9] The filling factor $f = W/P$ of GRAs is fixed at 0.5 in our model. The resonance frequency $\omega_{p,j}$ of graphene plasmons in GRAs is expressed as[14]

$$\omega_{p,j} = \sqrt{\frac{D_j}{\eta\varepsilon_{eff}\varepsilon_0 W_j}}. \tag{4}$$

Here, $\varepsilon_{eff} = ({n_1}^2 + {n_2}^2)/2 = ({n_2}^2 + {n_3}^2)/2$ is the effective permittivity of media surrounding the GRAs, ε_0 is the vacuum permittivity, and W_j is the ribbon width of GRAs. η is a fitting parameter deduced from the simulated results, and the subsequent simulations demonstrate $\eta = 2.45$ in our model. It is found that the GRAs/SiO_2/GRAs structure is exactly a FP oscillator, in which the GRAs can be regarded as the two mirrors of traditional FP cavity. In particular, the Fresnel coefficients of mirrors can be dynamically tuned by gate voltages due to the tunability of optical conductivity of the GRAs. According to Eqs. (1)–(4), the transmittance of graphene-integrated FP microcavity is derived as

$$T = \left(\frac{4n_1 n_2}{(n_2 + n_1 + Z_0\sigma_1)(n_2 + n_1 + Z_0\sigma_2)e^{-i\varphi} - (n_2 - n_1 - Z_0\sigma_1)(n_2 - n_1 - Z_0\sigma_2)e^{i\varphi}} \right)^2. \tag{5}$$

Based on the aforementioned theoretical analyses, numerical investigations are further performed by using finite-difference time-domain (FDTD) method. In the simulations, monolayer graphene sheet is modeled as a 0.5-nm-thick (Δ) anisotropic material: isotropic in the plane of sheet and no-dispersive out of the plane, whose permittivity can be described by a diagonal tensor.[22] The in-plane component is $\varepsilon_{xx} = \varepsilon_{yy} = 2.5 + i\sigma_g/(\varepsilon_0\omega\Delta)$ and the out-of-plane component is $\varepsilon_{zz} = 2.5$, wherein $\sigma_g = iD/(\pi(\omega + i\Gamma))$ is the Drude optical conductivity of graphene under condition of only intraband transition within the random-phase approximation.[16,23] The maximum mesh size inside the graphene layer is set as $\Delta x = \Delta y = 0.5$ nm and $\Delta z = 0.05$ nm, which is small enough to ensure the numerical convergence of the results.[23] The excitation source is the mid-infrared plane wave and incidents normally to the surface of GRAs with electric field vector perpendicular to graphene ribbons.[13–15]

One can see that the transmission depends strongly on the incident frequency ω, separation h, ribbon width W, and Fermi energy E_F of GRAs. We first consider the FP microcavity with the same W and E_F in two GRAs according to Eq. (5). Figure 2(a) illustrates the theoretically calculated transmission dependence on ribbon width as a function of frequency. It is found that there exists a profound dip $(T = 0)$ on transmission spectrum, which originates from the plasmon resonances in graphene ribbons.[13–15] The corresponding FDTD numerical results in the inset of Fig. 2(a) show the near-perfect absorption of incident wave around 33 terahertz (THz), which paves the way of strong amplitude modulations.[24] The dependence on Fermi energy is also calculated in Fig. 2(b), indicating the blue shift of transmission dip with the increasing of Fermi energy. The electrical control of the graphene-integrated FP microcavity through electrostatic gating is here discussed. The Fermi

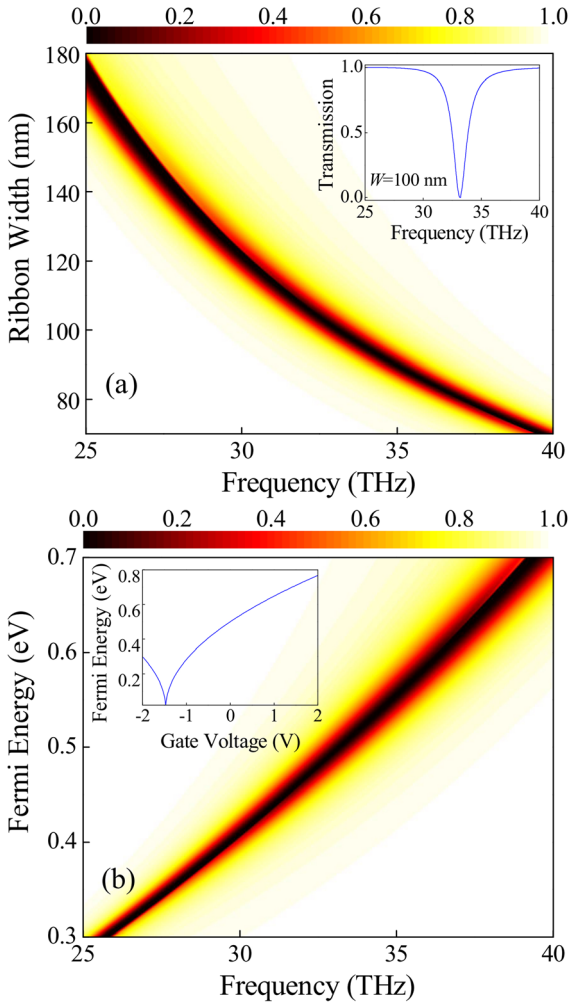

FIG. 2. (a) Transmission dependence on ribbon width as a function of frequency with $E_{F,1} = E_{F,2} = 0.5\,\text{eV}$. The inset shows the numerical results of transmission at $W_1 = W_2 = 100\,\text{nm}$. (b) Transmission dependence on Fermi energy as a function of frequency with $W_1 = W_2 = 100\,\text{nm}$. The inset shows the calculated Fermi energy as a function of gate voltage using a parallel-plate capacitor model. In the investigations, the separation h is fixed at 3 μm.

energy $E_F(V_g)$ of GRAs is estimated using a parallel-plate capacitor model as[11,12]

$$|E_F(V_g)| = \hbar v_F \sqrt{\pi |\alpha_c V_g - n_{s0}|}. \quad (6)$$

Here, $n_{s0} = 1.8 \times 10^{13}\,\text{cm}^{-2}$ (corresponding to Fermi energy of 0.5 eV) is the natural doping of graphene and $\alpha_c = 1.2 \times 10^{13}\,\text{cm}^{-2}\,\text{V}^{-1}$ is the capacitor constant of ion-gel gating.[11,13] The calculated Fermi energy as a function of gate voltage is plotted in the inset of Fig. 2(b).

Successively, the performances of the FP microcavity with different Fermi energies (i.e., gate voltages) in two GRAs are investigated theoretically and numerically. As shown in Fig. 3(a), interestingly, a transparency peak emerges around the original transmission dip when the gate voltages of two GRAs are slightly detuned. This phenomenon, being similar to the PIT effect in metallic plasmonic FP systems, is attributed to the constructive interference between the reflected waves by two mirrors.[25,26] Moreover, by varying the ribbon width, the PIT peaks can be generated over a wide frequency range from 25 to 40 THz. The FDTD simulations coincide well with the calculated results in Fig. 3(a). To further illustrate the physical mechanism of the PIT effect in our model, the field distributions at frequencies of the transmission dips and peak are presented in Figs. 3(b)–3(d). With the same parameters as that in the inset of Fig. 3(a), the resonance frequencies of GRA1 and GRA2 are located at 32.49 and 33.86 THz, respectively. As depicted in Figs. 3(b) and 3(d), when the excitation frequency is 32.49 or 33.86 THz, the local graphene plasmon resonances are excited in the individual GRAs and the excitation wave is strongly reflected. For the transparency frequency, the two partially resonant GRAs form a FP oscillator, and the excitation wave can pass through the graphene-based oscillator, exhibiting a PIT-like effect, as shown in Fig. 3(c). The field distributions are consistent with the transmission spectrum in Fig. 3(a).

In accordance with the FP oscillations, the round-trip phase is controlled by the optical path difference between two mirrors. Therefore, the transmission properties can be changed by adjusting the separation h of the two GRAs. Figure 4 reveals the transmission spectra at various values of h resulting from the FDTD simulations and theoretical calculations. It is found that the transmission spectra exhibit typical features of the FP oscillations, for instance, periodic, asymmetric, and blue-/red-shifted peaks with the variation of h.[25] A symmetric spectrum with the highest transmittance ~92% is achieved when $h = 3.12\,\mu\text{m}$. The periodic evolution of transmission spectrum with the separation h is theoretically calculated and illustrated in Fig. 4(b) to further clarify the FP-like spectral features of the graphene-integrated FP microcavity.

Once the fabrication of the proposed microcavity is completed, the performance of the proposed microcavity can also be flexibly adjusted by gate voltages. As a proof of applications, here, a frequency-selective electro-optic shutter is demonstrated by taking advantage of the PIT effect in the proposed configuration. Figure 5(a) shows that the microcavity can realize modulating of ON and OFF states for the incident optical signal at frequency of 33.16 THz, and most importantly, the intensity modulation depth (i.e., ON/OFF ratio) exceeds 90%. In addition, this shutter works perfectly well over a wide band frequency in the mid-infrared regime, as shown in Fig. 5(b). In the frequency region we considered, the ON/OFF ratios and quality factors are lager than ~86% and ~38, respectively.

In conclusion, we have demonstrated that integrating electrically gated GRAs onto a dielectric spacer allows the realization of strong optical modulations. The graphene-integrated microcavity is exactly a FP oscillator with electrically tunable Fresnel coefficients, and its performance is thus controllable by the gate voltages. By optimizing the physical parameters, an extremely strong optical modulation (~90%) is observed in the mid-infrared based on the PIT effect, which is much larger than that of Ref. 17. It is expectable that the modulation depth can be further improved by higher carrier mobility of graphene.[5,12,13] Additionally, the proposal can be scaled to a wider range from the mid-infrared to THz. The potential for extremely large modulation depth and broadband operation range promises the development of active high-performance spatial light modulators in chip-integrated photonic circuits.

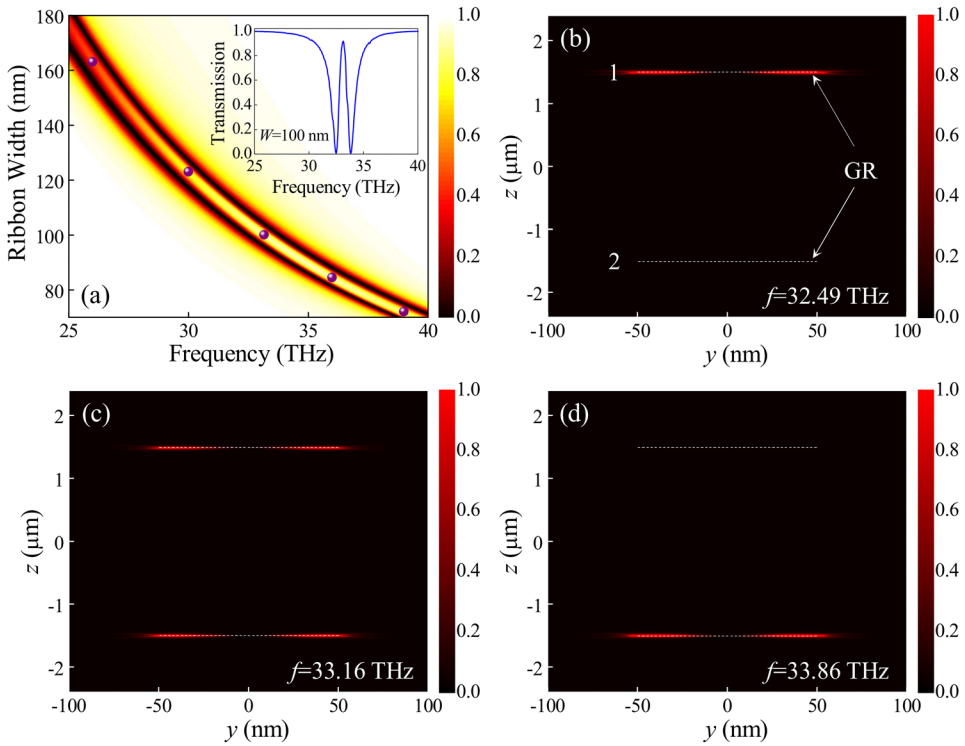

FIG. 3. (a) Transmission dependence on ribbon width as a function of frequency with different gate voltages $V_{g1} = -116$ mV (0.48 eV) and $V_{g2} = 120$ mV (0.52 eV). The five purple spheres display the numerical resonance frequencies of PIT peaks at $W = 72$, 85, 100, 123, and 163 nm. The inset shows the numerical transmission spectrum at $W = 100$ nm. (b)–(d) Numerical field distributions ($|E_z|^2$) of graphene plasmon resonances in a unit cell of the graphene-integrated FP microcavity ($W = 100$ nm) with the excitation frequency at 32.49 (left dip), 33.16 (PIT peak), and 33.86 THz (right dip), respectively. The white dashed lines indicate the locations of GR 1 and 2. In the investigations, the separation h is fixed at 3 μm.

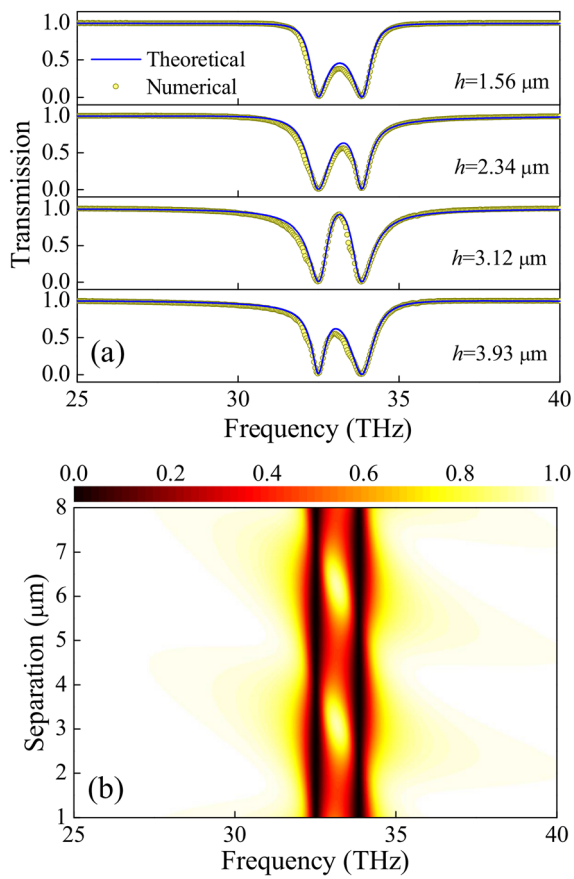

FIG. 4. (a) Numerical (circles) and theoretical (solid curves) transmission spectra with different separations h between GRA1 and GRA2. (b) Evolution of transmission spectrum as a function of separation h. The other parameters are $V_{g1} = -116$ mV, $V_{g2} = 120$ mV, and $W_1 = W_2 = 100$ nm.

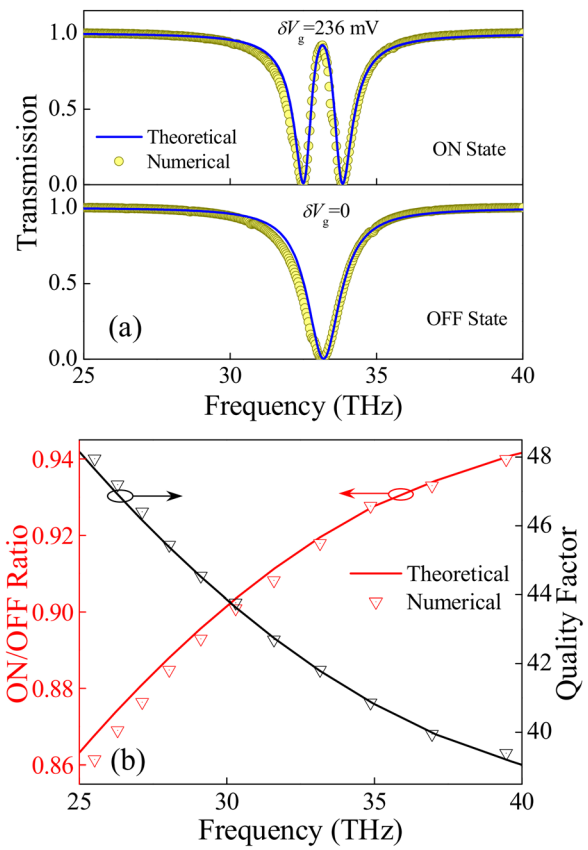

FIG. 5. (a) Demonstration of an electro-optic shutter based on the graphene-integrated FP microcavity. OFF state: when $\delta V_g = 0$, $T = 0$ at 33.16 THz. ON state: when $\delta V_g = 236$ mV, $T = 92.5\%$ at 33.16 THz. The detuning of gate voltages is defined by $\delta V_g = V_{g2} - V_{g1}$. (b) ON/OFF ratio and quality factor of shutter over a wide frequency range from 25 to 40 THz. The other parameters are derived from Eqs. (2) to (6).

This work was supported by the National Natural Science Foundation of China under Grant Nos. 10874239, 10604066, and 61223007.

[1]K. S. Novoselov, A. K. Geim, S. V. Morozov, D. Jiang, Y. Zhang, S. V. Dubonos, I. V. Grigorieva, and A. A. Firsov, Science **306**, 666 (2004).
[2]F. Bonaccorso, Z. Sun, T. Hasan, and A. C. Ferrari, Nat. Photonics **4**, 611 (2010).
[3]Q. Bao and K. P. Loh, ACS Nano **6**, 3677 (2012).
[4]M. Liu, X. Yin, E. Ulin-Avila, B. Geng, T. Zentgraf, L. Ju, F. Wang, and X. Zhang, Nature **474**, 64 (2011).
[5]B. Sensale-Rodriguez, R. Yan, M. M. Kelly, T. Fang, K. Tahy, W. S. Hwang, D. Jena, L. Liu, and H. G. Xing, Nat. Commun. **3**, 780 (2012).
[6]F. Xia, T. Mueller, Y.-M. Lin, A. Valdes-Garcia, and P. Avouris, Nat. Nanotechnol. **4**, 839 (2009).
[7]X. Gan, R.-J. Shiue, Y. Gao, I. Meric, T. F. Heinz, K. Shepard, J. Hone, S. Assefa, and D. Englund, Nat. Photonics **7**, 883 (2013).
[8]K. F. Mak, M. Y. Sfeir, Y. Wu, C. H. Lui, J. A. Misewich, and T. F. Heinz, Phys. Rev. Lett. **101**, 196405 (2008).
[9]S. Thongrattanasiri, F. H. L. Koppens, and F. J. García de Abajo, Phys. Rev. Lett. **108**, 047401 (2012).
[10]Q. Ye, J. Wang, Z. Liu, Z.-C. Deng, X.-T. Kong, F. Xing, X.-D. Chen, W.-Y. Zhou, C.-P. Zhang, and J.-G. Tian, Appl. Phys. Lett. **102**, 021912 (2013).
[11]A. Majumdar, J. Kim, J. Vuckovic, and F. Wang, Nano Lett. **13**, 515 (2013).
[12]W. Gao, J. Shu, K. Reichel, D. V. Nickel, X. He, G. Shi, R. Vajtai, P. M. Ajayan, J. Kono, D. M. Mittleman, and Q. Xu, Nano Lett. **14**, 1242 (2014).
[13]L. Ju, B. Geng, J. Horng, C. Girit, M. Martin, Z. Hao, H. A. Bechtel, X. Liang, A. Zettl, Y. R. Shen, and F. Wang, Nat. Nanotechnol. **6**, 630 (2011).
[14]H. Yan, X. Li, B. Chandra, G. Tulevski, Y. Wu, M. Freitag, W. Zhu, P. Avouris, and F. Xia, Nat. Nanotechnol. **7**, 330 (2012).
[15]H.-S. Chu and C. H. Gan, Appl. Phys. Lett. **102**, 231107 (2013).
[16]Z. Fang, S. Thongrattanasiri, A. Schlather, Z. Liu, L. Ma, Y. Wang, P. M. Ajayan, P. Nordlander, N. J. Halas, and F. J. García de Abajo, ACS Nano **7**, 2388 (2013).
[17]H. Cheng, S. Q. Chen, P. Yu, X. Y. Duan, B. Y. Xie, and J. G. Tian, Appl. Phys. Lett. **103**, 203112 (2013).
[18]A. N. Grigorenko, M. Polini, and K. S. Novoselov, Nat. Photonics **6**, 749 (2012).
[19]B. Sensale-Rodriguez, T. Fang, R. Yan, M. M. Kelly, D. Jena, L. Liu, and H. G. Xing, Appl. Phys. Lett. **99**, 113104 (2011).
[20]B. Sensale-Rodriguez, R. Yan, M. Zhu, D. Jena, L. Liu, and H. G. Xing, Appl. Phys. Lett. **101**, 261115 (2012).
[21]T. Stauber, N. M. R. Peres, and A. K. Geim, Phys. Rev. B **78**, 085432 (2008).
[22]W. Gao, J. Shu, C. Qiu, and Q. Xu, ACS Nano **6**, 7806 (2012).
[23]M. Jablan, H. Buljan, and M. Soljačić, Phys. Rev. B **80**, 245435 (2009).
[24]Y. Gong, Z. Li, J. Fu, Y. Chen, G. Wang, H. Lu, L. Wang, and X. Liu, Opt. Express **19**, 10193 (2011).
[25]H. Lu, X. M. Liu, and D. Mao, Phys. Rev. A: At., Mol., Opt. Phys. **85**, 053803 (2012).
[26]X. Y. Yang, X. Y. Hu, Z. Chai, C. C. Lu, H. Yang, and Q. H. Gong, Appl. Phys. Lett. **104**, 221114 (2014).